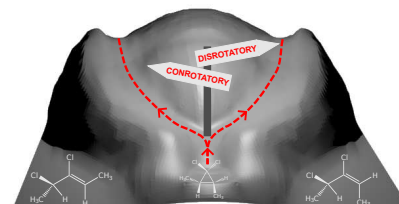


# Force-induced Catastrophes on Energy Landscapes: Mechanochemical Manipulation of Downhill and Uphill Bifurcations Explains Ring-opening Selectivity of Cyclopropanes

Miriam Wollenhaupt,<sup>1</sup> Christoph Schran,<sup>1</sup> Martin Krupička,<sup>1, a)</sup> and Dominik Marx<sup>1, b)</sup>  
*Lehrstuhl für Theoretische Chemie, Ruhr-Universität Bochum, 44780 Bochum, Germany*

(Dated: 30 March 2021)

The mechanochemistry of ring-opening reactions of cyclopropane derivatives turns out to be unexpectedly rich and puzzling. After showing that a rare so-called uphill bifurcation in the case of *trans-gem*-difluorocyclopropane turns into a downhill bifurcation upon substitution of fluorine by chlorine, bromine and iodine in the thermal activation limit, the dichloro derivative is studied systematically in the realm of mechanochemical activation. Detailed exploration of the force-transformed potential energy surface of *trans-gem*-dichlorocyclopropane in terms of Dijkstra path analysis unveils a hitherto unknown topological catastrophe where the global shape of the energy landscape is fundamentally changed. From thermal activation up to moderately large forces, it is an uphill bifurcation that decides about dis- versus conrotatory ring-opening followed by separate transition states along both pathways. Above a critical force, the two distinct transition states merge to yield a single transition state such that the decision about the dis- versus conrotatory ring-opening process is taken at a newly established downhill bifurcation. The discovery of a force-induced qualitative change of the topology of a reaction network vastly transcends the previous understanding of the ring-opening reaction of this species. It would be astonishing to not discover a wealth of such catastrophes for mechanochemically activated reactions which will greatly extend the known opportunities to manipulate chemical reaction networks.



Keywords: Mechanochemistry, Woodward-Hoffmann rules, Electrocyclic reactions, Reaction mechanisms

## I. INTRODUCTION

Chemists usually think of a transition state as a stationary-point structure connecting a reactant with one product state, thus linking two minima on the potential energy surface (PES). However, it is well established that PESs can also feature bifurcations which open the opportunity to explore pathways that start at the same reactant, share the same path for a while, but lead to more than one reaction channel at some point, thus connecting the same reactant to more than one product state.<sup>1,2</sup> As will be described in more detail below, such bifurcations along a reaction pathway usually occur after a transition state, leading to what is called “downhill bifurcations”, but in rare cases so-called “uphill bifurcations” occur before even reaching a transition state. Chemical substitution represents the classic way to change the PES and, thus, to manipulate also such bifurcations. Within this traditional approach, the underlying energy landscape gets changed due to steric and other electronic effects which can offer the possibility to arrive at new reaction

pathways.<sup>3-6</sup> Obviously, these manipulations can only be realized in a discrete manner by exchanging one atom or a group of atoms by another one.

In stark contrast, it is well established in the framework of covalent mechanochemistry<sup>7-10</sup> that potential energy landscapes, i.e. PESs, can be *continuously* distorted as a result of applying external forces to molecules.<sup>9,11,12</sup> As reviewed in depth from the experimental<sup>8</sup> and computational<sup>9</sup> viewpoints, mechanochemical activation can lead to different products from the usual thermally or photochemically favored ones, if sufficiently large forces are applied. In the following, we will explore in detail for a specific system class, namely for cyclopropanes, how bifurcations can be systematically tuned by means of applying such mechanical forces to molecules.

A scenario that is rather often found in the literature are bifurcations in the post-transition state region as sketched in Fig. 1(a), which are usually denoted as downhill bifurcations. The common pathway that starts in the reactant state ascends in energy (not visible in the figure) until it reaches the transition state  $TS_{Rct}$  and from there on it exclusively moves downhill in energy (from top to bottom in Fig. 1(a)) as in any standard chemical reaction. At some distinct point upon moving toward the product state, however, the common path arrives at the bifurcation where it splits into two separate pathways which ultimately lead to two different minima denoted as  $Prod_1$

<sup>a)</sup>Present Address: Department of Organic Chemistry, University of Chemistry and Technology, Technická 5, 16628 Prague, Czech Republic

<sup>b)</sup>Electronic mail: [dominik.marx@rub.de](mailto:dominik.marx@rub.de)

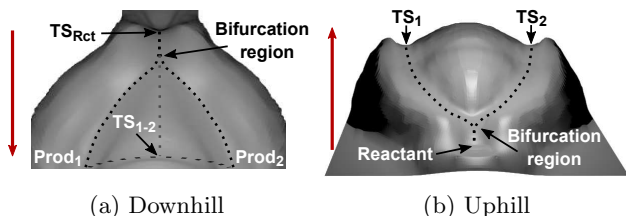


FIG. 1: Schematic potential energy surfaces with downhill (a) and uphill (b) bifurcations. The reactions in (a) and (b) proceed from top to bottom and from bottom to top, respectively, as indicated by the two vertical arrows to the left of the landscapes.

and  $\text{Prod}_2$  in Fig. 1(a). These two products, in turn, are connected by a second transition state,  $\text{TS}_{1-2}$ , which is related to the direct interconversion of Product 1 and 2. Thus, a PES exhibiting a downhill bifurcation possesses two close-lying and consecutive transition states with no local minimum in between.

Much more seldomly found, and thus of considerable fundamental interest, are uphill bifurcations such as the one sketched in Fig. 1(b). An uphill bifurcation is best described by a reaction path that starts at the reactant minimum and leads uphill in energy while initially passing through a unique valley akin to any standard chemical reaction thereby moving from bottom to top in Fig. 1(b). At some specific point, however, the valley branches at the bifurcation *before* any transition state is reached and two new valleys with their own subsequent transition states, labeled as  $\text{TS}_1$  and  $\text{TS}_2$  in Fig. 1(b), emerge. Although downhill bifurcations are, for instance, well-established in the realm of thermal cycloaddition reactions,<sup>13,14</sup> uphill bifurcations are far less frequently described in the extant literature.<sup>15–19</sup> Indeed, this rare topological phenomenon has not been addressed at all in recent authoritative overview articles on reaction path bifurcations,<sup>1,2</sup> whereas a rigorous definition can be found in Ref. 20.

Mechanochemical ring-opening of cyclopropane derivatives (see Fig. 2) might be a good candidate reaction to search for force-induced bifurcation changes in view of various surprising findings in the recent literature.<sup>21–32</sup> In particular, *ab initio* molecular dynamics simulations at constant force revealed very puzzling behavior of *trans*-1,1-dichloro-2,3-dimethylcyclopropane upon disrotatory ring-opening at finite temperatures,<sup>23</sup> namely the preferential generation of two different diastereomers depending on the magnitude of the force (see Fig. 3 in Ref. 23); note that this reactant, which is (2*S*,3*S*)-1,1-dichloro-2,3-dimethylcyclopropane, is abbreviated in the literature by *trans-gem*-dichlorocyclopropane or by *trans-gDCC*. Spurred by the findings, we explored the force-transformed potential energy surfaces (FT-PES) of this cyclopropane derivative in more detail based on static isotensional calculations and discovered a qual-

itative change in the energetically preferred reaction channel.<sup>27</sup> Analyzing the Intrinsic Reaction Coordinates (IRC), we could show that disrotatory ring-opening, which is symmetry-allowed in the thermal limit at zero force, switches to the conrotatory process at forces exceeding about 1.6 nN (being symmetry-forbidden in the thermal activation limit).<sup>27</sup> Moreover, we demonstrated that the conrotatory mechanism does even exist down to zero force where it is symmetry-forbidden, albeit as a high-energy reaction channel.<sup>27</sup> These key computational findings<sup>27</sup> are in line with a subsequent publication on single-molecule force spectroscopy measurements.<sup>28</sup>

In this work, we significantly transcend the current knowledge by demonstrating that a system class as simple as cyclopropane derivatives indeed features not only downhill but also uphill bifurcations which can be manipulated systematically by applying mechanical forces. The *trans-gem*-dihalocyclopropanes being in the focus of the present study are able to undergo disrotatory and conrotatory ring-opening reactions together with subsequent halogen migration to one or the other neighboring carbon site within the three-membered ring as shown in Fig. 2. In case of the fluorine disubstituted system it is important to note that halogen migration corresponds to a higher-lying reaction channel than the experimentally observed ring-opening/closing process,<sup>33,34</sup> which we discuss in detail in Sec. 1.2 of the SI. Ring-opening with subsequent halogen migration leads to four product species in total which can be classified in terms of Woodward-Hoffmann (WH) allowed and forbidden electrocyclic reactions as a result of thermal activation together with the migration direction of the halogen. Upon mechanochemical activation, it will be unveiled that this system features fundamental topological phenomena since both contributions to the full reaction mechanism are connected to uphill/downhill bifurcations that can be tuned by external force. In order to set the stage, we initially investigate the disrotatory reactions of differently substituted dihalocyclopropanes which are the WH allowed processes upon thermal activation. We discover that the bifurcations deciding on the migration direction of the moving atom depend on the particular halogen, and thus that these bifurcations can indeed be manipulated by means of classic chemical substitution. For the total disrotatory and conrotatory reaction profile of *trans-gem*-dichlorocyclopropane we find both types of bifurcation to be present at zero force. The subsequent core part of our investigation is focused on how both the downhill and uphill bifurcations in the dichloro derivative can be manipulated by applying tensile forces to the two methyl substituents and, in addition, reveals catastrophes at specific critical force magnitudes.

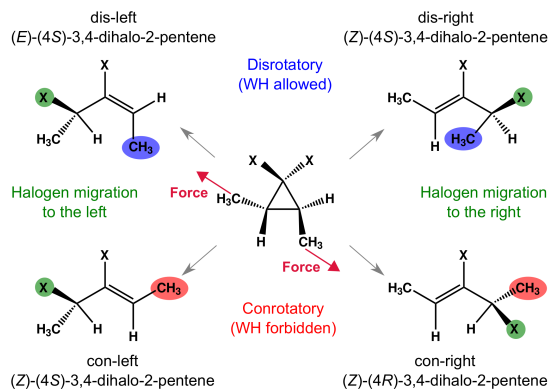


FIG. 2: The reactant species (i.e.  $(2S,3S)$ -1,1-dihalo-2,3-dimethylcyclopropanes a.k.a. *trans-gem*-dihalocyclopropanes or *trans-gDHC*) at the center and the corresponding four products in the corners are schematically depicted including their IUPAC nomenclature as well as our short hand notation that is used in the present work; see Sec. 1.1 in the SI for details regarding our nomenclature.

## II. RESULTS AND DISCUSSION

### A. Chemical Substitution of Cyclopropanes: From Fluorine to Iodine

As a first step toward investigating putative force-induced topology changes of the PES of cyclopropane derivatives, cf. Fig. 2, the bifurcation structures of the  $(2S,3S)$ -1,1-dihalo-2,3-dimethylcyclopropanes are analyzed in the usual thermal limit for the fluorine up to iodine disubstituted species. It is found that the difluorinated cyclopropane derivative exhibits two separate disrotatory transition states, one leading to what we call the fluorine-left-product whereas the other one connects to the fluorine-right-product (left and right being defined for the migration of the halogen within our reference frame as specified in Fig. S1 of the SI). These two transition states correspond to energetically higher-lying reaction pathways compared to the theoretically<sup>33</sup> predicted and experimentally<sup>34</sup> established ring-opening/closing reaction channels of this system as detailed in Sec. 1.2 of the SI. However, in the present case exactly these higher-lying reaction pathways of the ring-opening and subsequent fluorine migration processes are of fundamental interest in order to coherently compare the changes of the PES upon chemical substitution. The paths to these two first-order saddle points on the PES start at the same stationary point representing the reactant species and initially share the identical pathway, both structurally and energetically, when moving uphill (the energies along the corresponding IRCs are shown in Fig. S3 of the SI). At some specific point, however, an uphill bifurcation occurs where two distinct pathways emerge which evolve separately *via* their own transition states,

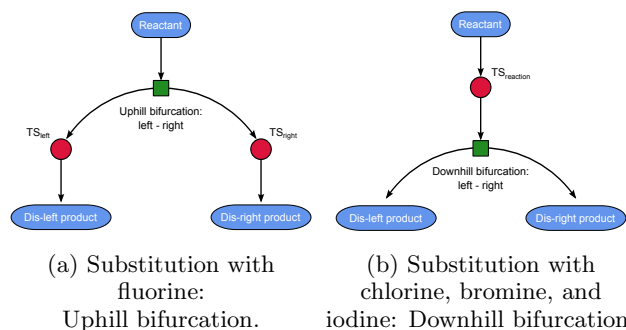


FIG. 3: Disrotatory reaction schemes depending on the dihalogen substitution of  $(2S,3S)$ -1,1-dihalo-2,3-dimethylcyclopropane in the thermal reference case (corresponding to the zero-force limit). Reactant and product minima, transition states, and bifurcations are depicted in blue, red and green, respectively.

$TS_{\text{left}}$  and  $TS_{\text{right}}$ , to two different stationary states being the respective disrotatory products, dis-left and dis-right, as illustrated in Fig. 3(a). This is exactly the scenario that has been discussed in the introduction with the help of Fig. 1(b) and therefore adds  $(2S,3S)$ -1,1-difluoro-2,3-dimethylcyclopropane to the few known chemical reactions that feature an uphill bifurcation.

In stark contrast to the difluoro species, substitution with chlorine, bromine and iodine leads to one common thermal disrotatory transition state,  $TS_{\text{reaction}}$ , and a subsequent downhill bifurcation such as the one sketched in Fig. 1(a) that decides about the direction of the migration of the moving halogen atom to the dis-left and dis-right product states.

Investigating the evolution of particular vibrational modes along IRCs has recently been successfully employed in order to analyze bifurcations,<sup>35</sup> although frequency analyses have to be interpreted carefully if the analyzed structure is not a stationary point on the PES. (see also Sec. 1.4 in the SI). In the present case, the evolution of the lowest two frequencies of the fluorine species along the IRC corresponding to the thermal disrotatory ring-opening reaction depicted in Fig. 4(a) is distinctly different from that of the chlorine (b), bromine (c) and iodine (d) disubstituted cyclopropane derivatives (which all look quite similar). Only one imaginary frequency is observed for disrotatory ring-opening of the difluoro species which is related to the fluorine-carbon stretch that belongs to the transition state of the overall reaction either along  $TS_{\text{left}}$  or  $TS_{\text{right}}$  toward the dis-left and dis-right product, respectively. The appearance of a single imaginary frequency along a reaction path that bifurcates, which is left/right fluorine migration in the present case as indicated using solid/dashed lines in Fig. 4(a), is a characteristic feature of the above-mentioned uphill bifurcation being in accord with the topology of Fig. 1(b).

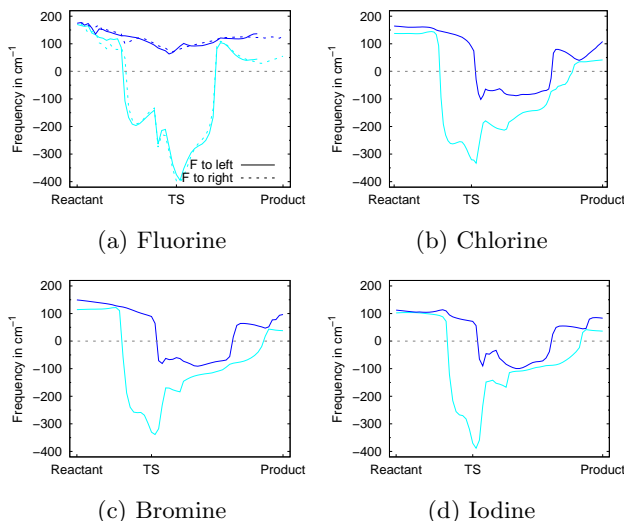


FIG. 4: Frequency analysis along the IRCs for disrotatory ring-opening of  $(2S,3S)$ -1,1-dihalo-2,3-dimethylcyclopropane derivatives subject to F (in panel a), Cl (b), Br (c), and I (d) disubstitution in the thermal reference case,  $F_0 = 0$  nN.

The evolution of the magnitude of the two lowest frequencies (negative values correspond to imaginary frequencies) is shown from the reactant state *via* the transition state to the product state.

In comparison to the fluorine case, the IRCs of the three other halogen derivatives feature more than one imaginary frequency. The same halogen-carbon stretch as in the fluorine case becomes most prominently imaginary when reaching the transition state, followed by one additional imaginary frequency that is directly related to the bifurcation that sets in after having passed  $TS_{\text{reaction}}$  when moving toward the products. It is essentially a bending vibration that is mainly related to the halogen left/right migration leading directly to the dis-left/right products and also describes the pathway that directly interconverts the dis-left and dis-right products via  $TS_{1-2}$ ; a detailed decomposition of this frequency analysis along the reaction paths for the chlorine case even for the force transformed PES can be found in Sec. 1.4.2 of the SI. This mode softening scenario agrees nicely with what is expected for a downhill bifurcation according to the generic PES in Fig. 1(a).

It is concluded that the difluorinated derivative of  $(2S,3S)$ -1,1-dihalo-2,3-dimethylcyclopropanes features one of the rarely observed uphill bifurcations upon thermally activated ring-opening followed by fluorine migration, while the dichlorine species is found to be the first one in this halogen homologous series that is characterized by a downhill bifurcation instead.

## B. Mechanochemistry of Dichlorocyclopropane: Force-induced Topology Changes

What has been unveiled in the previous section provokes the question if it might be possible to manipulate the bifurcation scenario of the dichlorocyclopropane species upon applying tensile stress with the aim to systematically influence the bifurcations. The remainder of this investigation will focus on that question by discussing the behavior of  $(2S,3S)$ -1,1-dichloro-2,3-dimethylcyclopropane as a function of constant force. Within this section, the global changes of the Born-Oppenheimer PES upon its force-transformation will be discussed, culminating in a topological catastrophe when reaching a specific critical force  $F_0^{\text{crit}}$ . Afterwards, the topological details in terms of how the uphill and downhill bifurcations and transition states shift as a function of mechanical force will be addressed separately for the respective parts of the FT-PES in the subsequent sections.

A broad understanding of the reaction behavior of this cyclopropane derivative under the influence of finite tensile forces has been obtained earlier based on dynamical explorations of wider regions of its energy landscape.<sup>23</sup> This included extensive mappings of multi-dimensional free energy surfaces for disrotatory ring-opening based on isotensional *ab initio* metadynamics as well as corresponding trajectory shooting simulations at a set of finite forces. Our subsequent static analysis of not only the disrotatory pathway as before,<sup>23</sup> but also of the conrotatory ring-opening along the corresponding IRCs as a function of the external force has brought deeper insights into the evolution of the electronic structure along these distinct reaction channels.<sup>27</sup>

In what follows, we combine these approaches in the sense that we now use isotensional *ab initio* molecular dynamics at several constant forces (within the EFEI approach as explained in the SI) in order to sample a vast ensemble of configurations with corresponding electronic energies. This allows us to generate the FT-PES as a function of force in a low-dimensional subspace which, in a second step, will be analyzed in terms of bifurcations and a catastrophe after adopting a static topology viewpoint; the generation of the FT-PES based on isotensional trajectories at a set of constant forces is explained in Sec. 1.5 of the SI. Three key structural parameters or collective variables (CVs) have been identified of being able to describe the important aspects of the processes in a reduced reaction subspace, see Fig. 5, rather than considering all internal degrees of freedom in full dimensionality. As the ring-opening and thus the bond breaking of the carbon-carbon bond within the three-membered cyclopropane ring constitutes a major part of the reaction, the corresponding distance (C2–C4) has been chosen as the first variable, CV1. Next, the dihedral angle of what we call the right methyl group is used as CV2 to discriminate between disrotatory and conrotatory trajectories. Last but not least, in order to differentiate between the

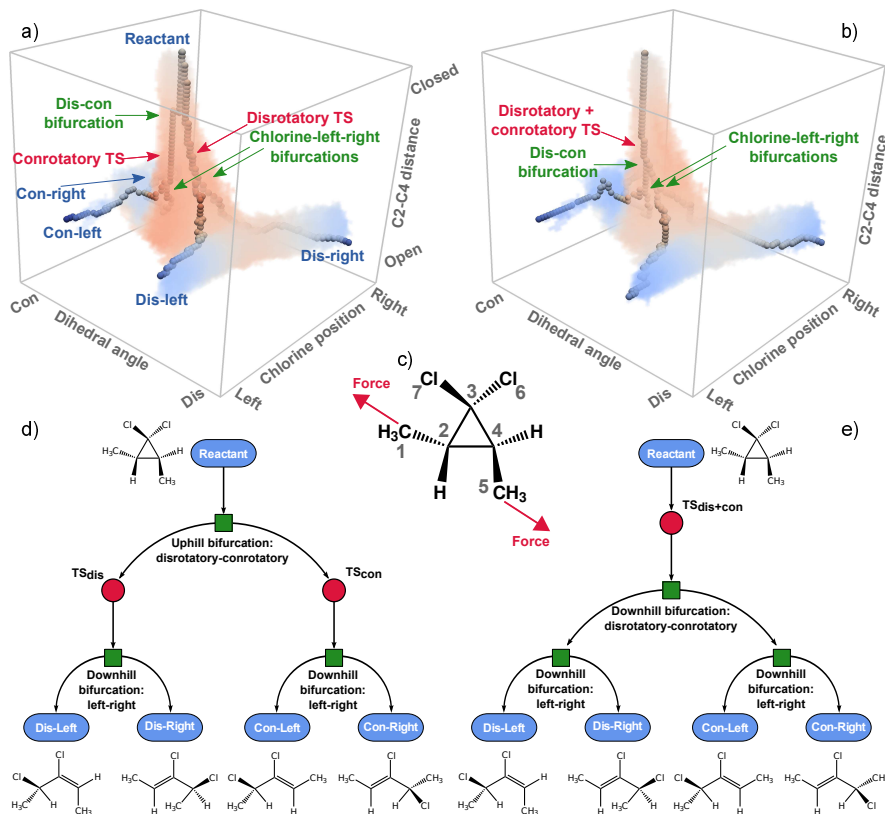


FIG. 5: Force-transformed effective potential energy surfaces (FT-ePES) at two different constant forces of  $F_0 = 1.0$  nN and  $F_0 = 2.0$  nN in panel (a) and (b), respectively, depicted in the reaction subspace spanned by the three selected collective variables (see text) as indicated. In addition, high/low energy parts of the FT-ePES are encoded using red/blue colors. The corresponding Dijkstra paths (see Sec. 1.6 in the SI for details) are included using a necklace representation. Panel (c) introduces the stereochemical formula of the (2*S*,3*S*)-1,1-dichloro-2,3-dimethylcyclopropane reactant, its atom numbering, and also indicates how the constant colinear force  $F_0$  acts on the two methyl groups. Panels (d) and (e) represent the two topologically distinct reaction schemes valid for zero (and moderate) forces in (d) and large forces in (e) corresponding to the FT-ePES of panel (a) and (b), respectively, and also display the stereochemical formulae of all products.

left and right products, the relative position of the migrating chlorine atom, which is C17, is employed as our third dimension, CV3. Therefore, the resulting FT-PES is not represented in the full-dimensional space defined in terms of all internal degrees of freedom, but in the three-dimensional (3D) reaction subspace spanned by the chosen collective variables, i.e. PES(CV1,CV2,CV3), which is why we call it the (force-transformed) “effective potential energy surface” (FT-) ePES. This dimensionality reduction from 39 down to only 3 variables turns out to be crucial not only to analyze, but also to visualize the force-induced changes of the bifurcations. On the FT-ePES, all four reaction paths from the reactant to the four possible products have been located by applying the Dijkstra algorithm,<sup>36</sup> thus providing what we call Dijkstra paths. Note that standard approaches to determine reaction pathways fail to map bifurcations which are usually not stationary points. The Dijkstra algorithm, in detail described in Sec. 1.6.1 of the SI, is therefore crucial to fully understand the changes of the ePES with respect

to force transformation.

Depending on the magnitude of the applied external force, we have found two topologically distinct reaction schemes that can connect the same reactant state with the four products. These scenarios correspond to uphill and downhill bifurcations according to panels (a,c) and (b,e) in Fig. 5 which are separated by a catastrophe that is triggered when using the magnitude of the external force as the control parameter in the spirit of catastrophe theory.<sup>37</sup> For clarity, we will first describe and explain the reaction course that is observed at zero force, i.e. in limit of a thermally activated process, which is a scenario that is still topologically valid at moderate finite forces. As depicted in the left part of Fig. 5, the processes leading to the four products share initially the same pathway on the FT-ePES. At some point, however, an uphill bifurcation deciding between disrotatory and conrotatory ring-opening occurs (denoted by “dis-con bifurcation” in panel (a) of Fig. 5) where the common path splits into two distinct ascending reaction channels before

any transition state is reached. After having passed this bifurcation that is still on the reactant side of the energy landscape, each of the paths climbs further up in energy and reaches its own transition state, denoted by con- and disrotatory TS in panel (a); note that irrespective of the occurrence of (uphill/downhill) bifurcations along a specific path the transition state remains always the (stationary first-order saddle) point of highest energy along that pathway whereas bifurcations do usually not correspond to stationary points and thus cannot be detected using the standard geometry optimizers in quantum chemistry packages. Only from the transition state on do the pathways descend in energy toward the products. One of the transition states corresponds to the disrotatory ring-opening reaction, whereas at the other the methyl groups rotate in the same fashion thus following a conrotatory mechanism.

Overall, we observe the following scenario at zero up to moderate forces, see Fig. 5(d). All four paths are degenerate before reaching the uphill bifurcation in the ascending part of the FT-ePES where they split into two pairs which remain degenerate all the way up to their transition states. After having passed their own transition state, thus being now on the descending side of the FT-ePES, they remain degenerate for a while before reaching the downhill bifurcation, where they finally split into left and right products. Hence, the four respective product channels represent a combination of con/disrotatory ring-opening and left/right chlorine migration that involve uphill and downhill bifurcations, respectively.

At forces higher than a specific critical value (denoted as  $F_0^{\text{crit}}$ , see next section for its quantification), the reaction scenario changes significantly as supported by the topology changes of the FT-ePES, see right panels of Fig. 5. In this high-force regime, again all four paths start in the reactant minimum but remain degenerate and thus do not bifurcate before they reach their common transition state. In contrast to the reaction route at sub-critical forces including the thermal activation limit, the FT-ePES in Fig. 5(b) does not contain any uphill bifurcation since a common transition state is reached directly after the ascending side of the energy landscape. After this joint transition state, however, a first downhill bifurcation can be found which leads to the splitting of the common pathway into two reaction channels (each being two-fold degenerate) corresponding to disrotatory and conrotatory ring-opening. Subsequently, yet another pair of downhill bifurcations occurs which decide on the left/right movement of the migrating chlorine atom (C17) after either con- or disrotatory ring-opening, and thus lift the remaining degeneracy by splitting the two paths for a second time.

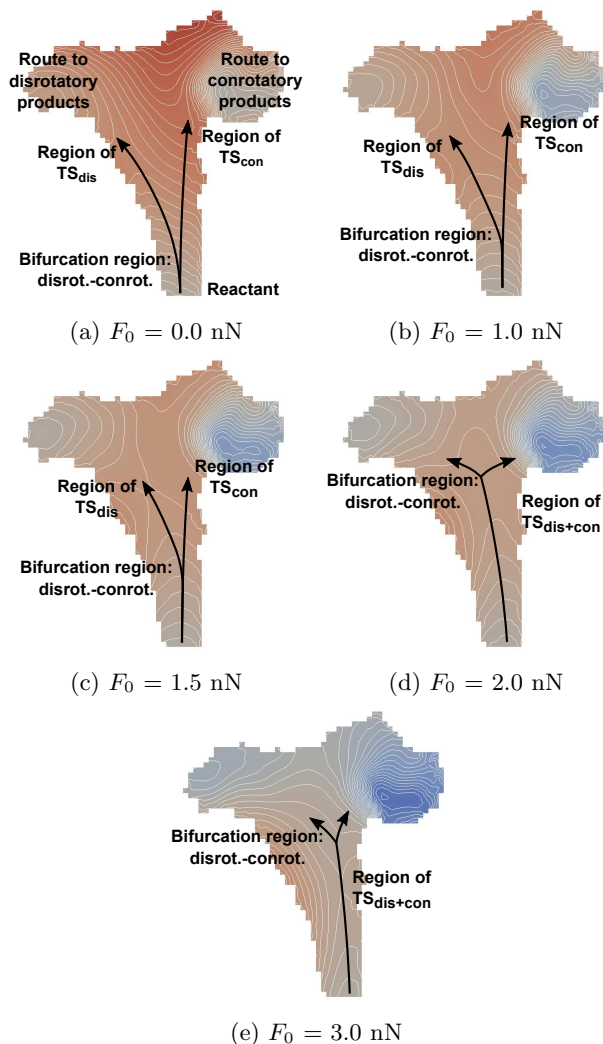


FIG. 6: Schematic illustration of the disrotatory and conrotatory Dijkstra paths on a set of 2D-slices of the 3D FT-ePES obtained at different constant forces from the thermally activated limit at 0 nN in panel (a) up to 3 nN in (e). The  $x$ -axis represents the dihedral angle of the methyl group (CV2) whereas the  $y$ -axis corresponds to the length of the breaking carbon-carbon bond (CV1). The reaction paths lead from the reactant region (bottom part of each panel) to the region of transition state/s (central part) and finally toward the dis- and conrotatory products (left and right upper parts, respectively); the arrow heads indicate the transition states whereas the branching points correspond to the bifurcations. The reactant energy is set to  $0 \text{ kcal mol}^{-1}$  for each FT-ePES and the depicted energy contour lines are separated by an equidistant spacing of  $2 \text{ kcal mol}^{-1}$  where red encodes increasing and blue decreasing energies compared to the reactant energy.

### C. Mechanochemistry of Dichlorocyclopropane: Reactant Regime

The quasi-3D representations of Fig. 5(a) and (b) are useful to visualize and discuss the global topology corresponding to the sub- and super-critical reaction scenarios, respectively, as they take place on the FT-ePES. Yet, only their reduction to specifically selected two-dimensional slices allows one to gain deeper insights as depicted in Fig. 6 for several constant forces from the thermal activation limit in panel (a) up to 3 nN in (e). These 2D-slices have been optimized in such a way that they cover the relevant parts of the 3D-PES with a focus on those regions where the bifurcations take place; one coordinate is essentially the breaking carbon-carbon bond and thus describes the first part of the reaction progress whereas the second coordinate is mostly the methyl dihedral and thus discriminates between the con- and disrotatory parts of the FT-ePES. The energy barriers for the reaction, being the difference between the reactant and the transition state regions, decrease with increasing mechanical forces (see Sec. 1.6.2 and 1.6.3 in the SI for reaction paths on the FT-ePES).

The force-dependent Dijkstra paths corresponding to the disrotatory and conrotatory ring-opening are schematically sketched on these 2D-slices using lines and arrows as collected in Fig. 6; see Sec. 1.6.1 in the SI for details on computing the Dijkstra paths numerically. At zero force, i.e. in the thermal reference case (a), all paths start at the same reactant but diverge readily afterwards. The left paths lead to the disrotatory side of the FT-ePES while the right paths connect the reactant to the conrotatory products; note that the left/right migration that decides about the final product after the ring-opening cannot be seen in this subspace of coordinates. As seen from the pattern of the contour lines, the initial part of the reaction channel is quite wide, which provides the possibility for an early divergence of the two paths that eventually lead to the dis- and conrotatory products. Clearly, the bifurcation between disrotatory and conrotatory ring-opening is positioned on the part of the FT-ePES with ascending energy, i.e. long before the two corresponding transition states are reached and, therefore, represents an uphill bifurcation. The two distinct transition states for the dis- and conrotatory reactions,  $TS_{\text{dis}}$  and  $TS_{\text{con}}$ , are located in the central left and right region about where the arrow heads are. Moreover, the two transition states are clearly separated from each other by an energy barrier which keeps these two reaction channels apart. This zero-force scenario is qualitatively valid up to a force of roughly 1.5 nN as shown in panel (c).

With increasing force, however, in the vicinity of the reactant, the reaction channel gets more narrow, which can be seen from the changing shape of the contour lines in the lower part moving from (a) to (b) to (c). More importantly, the two paths leading eventually to the dis- and conrotatory processes are found to increasingly share

the same part of the FT-ePES, which graphically shifts the bifurcation region upwards in the graphs upon increasing the force. Concurrently, the disrotatory and conrotatory transition states approach each other both structurally and energetically, implying that the energy barrier in between them gets systematically suppressed. The significant qualitative change with respect to the zero- to moderate-force scenario can most clearly be detected at a force of 3 nN, see Fig. 6(e). Now, the bifurcation into dis- and conrotatory ring-opening pathways occurs clearly after a common transition state  $TS_{\text{reaction}}$  which is shared by the two distinct ring-opening processes. This implies that the bifurcation into dis- and conrotatory ring-openings occurs thereafter and, thus, that it is a downhill bifurcation at such sufficiently large forces. In effect, the uphill bifurcation in the thermally activated reference case has been turned into a downhill bifurcation and thus has been shifted from the reactant (energy ascending) side of the energy landscape to the product (descending) side upon mechanochemical activation. In concert with this force-induced shift, the two formerly separated dis- and conrotatory transition states become confluent at sufficiently large forces and thus generate a single transition state that is common to both ring-opening reactions; note that the subsequent left/right bifurcation related to chlorine migration remains on the downhill (product) side irrespective of the force as will be discussed later. All these phenomena are already present at 2 nN in (d).

Based on this topological analysis, we conclude from the distortion of the FT-ePES that the catastrophe, which switches the topology from the reaction scenario valid in the thermal limit up to moderate forces (see Fig. 5(a) and (d)) to the large-force scenario (see Fig. 5(b) and (e)), occurs at a critical force  $F_0^{\text{crit}}$  that is bracketed by 1.5 and 2.0 nN. However, being close to the topological catastrophe, that part of the FT-ePES in panel (d), which covers the confluence of the two distinct transition states and the concurrent conversion of the uphill into a downhill bifurcation which needs to shift onto the other side of the new joint transition state, is very flat close to the critical force. This is borne out by analyzing the force-transformed energy profiles on the FT-ePES along the two Dijkstra paths corresponding to the dis- and conrotatory ring-opening processes, see Fig. S8(a) of the SI. As one can see, the conrotatory curve only slowly approaches the lower-lying disrotatory one upon increasing  $F_0$  such that the energy difference between the two processes eventually becomes insignificant before reaching  $F_0^{\text{crit}}$ . This energy difference is  $\approx 1.2$  kcal/mol at  $F_0 = 1.5$  nN and is on the order of only 0.1 kcal/mol at 1.8 and 1.9 nN before it vanishes at 2.0 nN, recall that the thermal energy,  $k_B T$ , corresponds to  $\approx 0.6$  kcal/mol at room temperature. Moreover, it is difficult to fully quantitatively analyze the catastrophe given the numerical inaccuracies due to the *ab initio* molecular dynamics sampling of the FT-PES in all 39 internal coordinates which underlies the construction of the coarse-grained effective

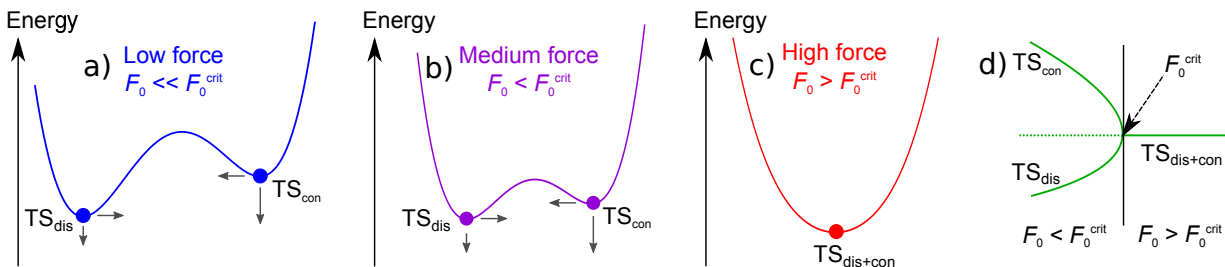


FIG. 7: Schematic representation of the force-induced distortions of the potential energy surface (FT-PES) in the region around the disrotatory ( $\text{TS}_{\text{dis}}$ ) and conrotatory ( $\text{TS}_{\text{con}}$ ) transition states. The cut through the FT-PESs is chosen to be perpendicular to the pathways *via* both  $\text{TS}_{\text{dis}}$  and  $\text{TS}_{\text{con}}$  which implies that the transition states appear as minima along the  $x$ -axis in this scheme whereas the central barrier is the one that energetically separates the two distinct pathways. Increasing the magnitude of the external force  $F_0$  transforms the topology of the energy landscape from the one characterizing the sub-critical regime sketched in (a) and also in (b) to that in the super-critical limit depicted in (c). The rightmost diagram (d) visualizes as a function of the control parameter  $F_0$  the change of topology upon increasing the force beyond its critical value,  $F_0 = F_0^{\text{crit}}$ , where the topological catastrophe occurs.

energy landscape, FT-ePES, in terms of only 3 collective variables. Last but not least, it is the full-dimensional FT-PES (and not the reduced-dimensionality treatment in terms of the FT-ePES that we introduced in order to access the rather complex bifurcation topology and its change at a function of force) which determines  $F_0^{\text{crit}}$ . The former has been analyzed previously<sup>27</sup> in terms of IRCs based on static isotensional quantum chemical calculations and is reproduced in Fig. S8(b) of the SI. As found for the Dijkstra paths in panel (a), the IRCs on the FT-PES start to come close at around 1.5 nN, where the conrotatory pathway is about 0.8 kcal/mol above the disrotatory one, before they essentially meet around 1.6 nN (where the corresponding energy difference is decreased to only  $\approx 0.3$  kcal/mol whereas no disrotatory transition state could be optimized at 1.7 nN and beyond). Based on this discussion, we conclude that the topological catastrophe occurs at a critical force close to  $F_0^{\text{crit}} = 1.6$  nN.

#### D. Analysis of the Catastrophe on the Force-transformed PES

With the help of catastrophe theory,<sup>37</sup> the shift and the confluence of the disrotatory and conrotatory transition states of the dichlorocyclopropane species as a result of applying constant mechanical forces can be viewed as a topological problem,<sup>12</sup> as already computationally exploited by us<sup>38</sup> quite some time back for another mechanochemical reaction. The key idea is that the systematic distortion of the usual Born-Oppenheimer PES as a result of its force transformation that yields the FT-PES can not only lead to quantitative changes for instance of activation or reaction energies, but can also induce qualitative changes of the FT-PES compared to the zero force (Born-Oppenheimer) PES; see Sec. 4.3 in Ref. 9 for a review of these concepts. These force-induced qualitative changes of the energy landscape correspond to a switching between different topologies of the FT-PES

at some specific force value,  $F_0^{\text{crit}}$ , thus the magnitude of the applied force is identified to be the “control parameter” in the language of catastrophe theory,<sup>38</sup> whereas the catastrophe itself is the sudden change of topology upon reaching  $F_0^{\text{crit}}$ .

The situation that we disclosed herein for dichlorocyclopropane is visualized with the help of Fig. 7 in terms of simplified cuts through the FT-PES. At forces smaller than  $F_0^{\text{crit}}$ , an uphill bifurcation leads to separate pathways for dis- and conrotatory ring-opening to which the two distinct transition states that are shown in panel (a), i.e.  $\text{TS}_{\text{dis}}$  and  $\text{TS}_{\text{con}}$ , correspond to. Increasing the mechanical force  $F_0$  leads to systematic shifts of  $\text{TS}_{\text{dis}}$  and  $\text{TS}_{\text{con}}$  in both energy and relative position within the energy landscape as qualitatively revealed when comparing panel (b) to (a). The activation energy associated to both pathways is gradually lowered upon increasing the applied external force, which is the usual mechanochemical activation due to suppressing the activation barrier w.r.t. the initial state *at the same force*. Thus, both TSs get lower in energy (relative to the reactant state serving as the reference) for larger  $F_0$ , but the conrotatory pathway is more susceptible to force which implies that the energy of  $\text{TS}_{\text{con}}$  decreases more quickly compared to  $\text{TS}_{\text{dis}}$  as symbolized by the length of the downward-pointing vertical arrows in panels (a) and (b). Concurrent to the lowering of the relative energy is also a confluence in configuration space, i.e. the two TSs move toward each other upon increasing  $F_0$  as encoded by the two horizontal arrows in these panels. At forces greater than  $F_0^{\text{crit}}$ , the two individual transition states have merged as depicted in (c) of Fig. 7 and form one joint transition state ( $\text{TS}_{\text{dis+con}}$ ) that is common to both reaction pathways (which eventually lead to dis- and conrotatory ring-opening after having passed the resulting downhill bifurcation, *vide infra*). Once  $\text{TS}_{\text{con}}$  and  $\text{TS}_{\text{dis}}$  are confluent and  $\text{TS}_{\text{dis+con}}$  has emerged, the two distinct uphill dis/conrotatory pathways including the underlying uphill bifurcation vanish as well. The resulting (local) cusp

catastrophe occurs right at  $F_0 = F_0^{\text{crit}}$  as visualized in panel (d) of Fig. 7 as a function of the continuous control parameter  $F_0$ .

### E. Mechanochemistry of Dichlorocyclopropane: Product Regime

After having discussed how the reaction channels originating in the reactant state split into dis- and conrotatory ring-opening processes below and above the catastrophe at  $F_0^{\text{crit}}$ , we finally turn to the analysis of the decision about chlorine left/right migration in terms of the FT-ePES which takes place in the product regime of the energy landscape. The 2D-slices on the product side of the disrotatory reaction region in Fig. 8 are oriented in such a way that the horizontal axis corresponds to the Cl position that nicely indicates left/right migration of Cl7, whereas the vertical axis results from a suitable combination of the distance of the breaking carbon-carbon bond and the methyl dihedral. In the following digression, we will concentrate on the bifurcation between dis-left- and dis-right-products, because the corresponding bifurcation on the conrotatory part of the FT-ePESs is essentially symmetric due to the underlying structural symmetries along this ring-opening channel, which are not broken by applying colinear external forces at the two methyl groups.

In the thermal reference case at 0 nN, the disrotatory transition state is located in the top part of the 2D-slice from there on the reaction paths evolve down in energy, see Fig. 8(a). The reaction channel in the middle part of the shown FT-ePES is relatively flat in the direction perpendicular to the course of the reaction, thus facilitating the structural separation of the two paths toward left and right migration. The resulting dis-left- and dis-right products in the bottom left/right corners of the FT-ePES are separated by the second transition state,  $\text{TS}_{\text{left/right}}$  (being analogous to the generic  $\text{TS}_{1-2}$  depicted in panel (a) of Fig. 1), that is clearly visible in the bottom-middle area in terms of the pattern of the contour lines.

As expected, the zero-force ePES gets distorted both in energy and shape due to the application of the tensile force to the methyl groups. With increasing force, the bifurcation area becomes flatter, which can be easily estimated by the decreasing number of contour lines when going from (a) to (b) etc. Furthermore, the position of the second transition state, which directly connects the dis-left to the dis-right product, shifts when applying a mechanical force. The second transition state (region) is located to a greater extent close to the center of the bifurcation area, making the surface more symmetric. Thus, in the case of a sufficiently large force and at finite temperatures, the force-transformed energy landscape, FT-ePES, would lead to a higher amount of the dis-right product compared to the thermal situation at zero force. Clearly, after the catastrophe on the reactant side of the

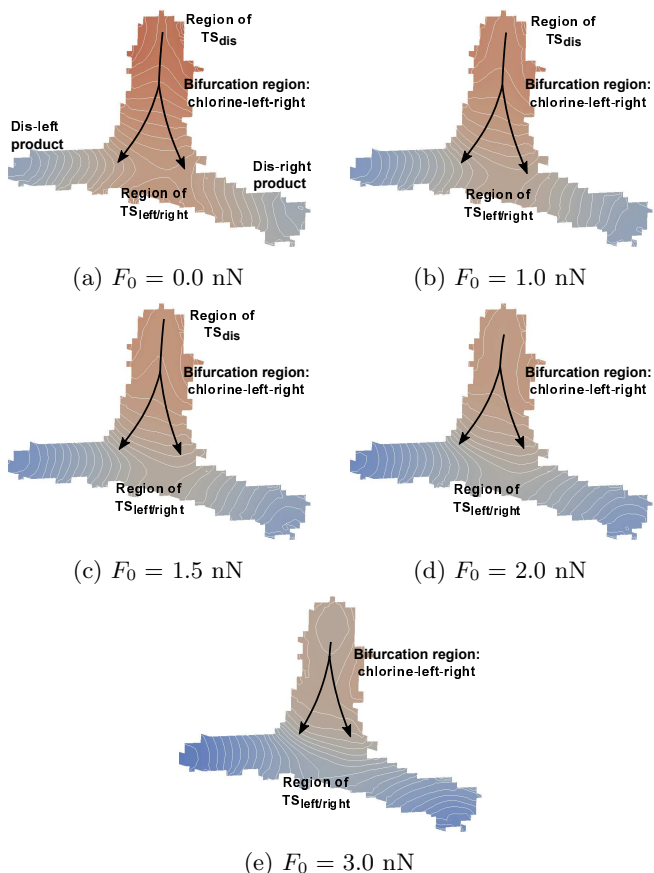


FIG. 8: Schematic illustration of the Dijkstra paths for left/right migration of chlorine after disrotatory ring-opening on a set of 2D-slices of the 3D FT-ePES obtained at different constant forces from the thermally activated limit at 0 nN in panel (a) up to 3 nN in (e).

The  $x$ -axis corresponds to the Cl position (CV3) whereas the  $y$ -axis is a suitable combination of the length of the breaking carbon-carbon bond (CV1) and the methyl dihedral (CV2). Starting at the disrotatory transition state (top part of each panel), the reaction pathways lead down in energy toward the left-right downhill bifurcation (central part) that connect to the dis-left and dis-right final products (left and right bottom parts, respectively). The reactant energy is set to  $0 \text{ kcal mol}^{-1}$  for each FT-ePES and the depicted energy contour lines are separated by an equidistant spacing of  $2 \text{ kcal mol}^{-1}$  where red encodes increasing and blue decreasing energies compared to the reactant energy.

energy landscape occurred, i.e. at forces exceeding  $F_0^{\text{crit}}$ , the isolines in the top part of Fig. 8(d) and (e) do no longer correspond to a transition state as they did at the lower forces in panels (a) to (c).

Overall, it is found that the region of that downhill bifurcation which decides about the left/right direction of the migrating chlorine atom, Cl7, does only change in quantitative details when applying tensile forces to the

methyl groups, whereas the local topology of this part of the energy landscape remains invariant in agreement with the two disrotatory branches in the lower parts of panels (d) and (e) in Fig. 5 that connect to the dis-left and dis-right products.

### III. CONCLUSIONS AND OUTLOOK

It is well appreciated in the extant literature that dihalogenated cyclopropanes display unexpected chemistry upon mechanochemical ring-opening reactions. In an effort to shed light on this puzzle, we investigated in the first step of the present study the impact of halogen substitution on the thermally activated ring-opening process followed by halogen migration of (2*S*,3*S*)-1,1-dihalo-2,3-dimethylcyclopropanes in the case of F, Cl, Br, and I disubstitution. Surprisingly, the decision about the direction of halogen migration (called “left” and “right” for simplicity) in case of disrotatory ring-opening occurs in qualitatively different ways for this difluorinated cyclopropane compared to the homologous Cl, Br, and I species. For *trans-gem*-difluorocyclopropane, the left/right decision is governed by an uphill bifurcation followed by two separate transition states for each migration direction, whereas the disrotatory transition state is first surmounted in the other three cases followed by a downhill bifurcation into the left and right disrotatory products. This change in the bifurcation scenario is corroborated by vibrational mode analysis performed along the respective intrinsic reaction coordinates. Thus, chemical substitution is found to qualitatively change the potential energy landscape for the ring-opening of cyclopropanes.

In our second step, which is based on quantum mechanochemical computations at constant external forces, we discover that the topology of the energy landscape for mechanochemically activated ring-opening of *trans-gem*-dichlorocyclopropane is qualitatively different in the high force regime compared to low forces down to the thermal limit. In particular, an uphill bifurcation that decides about dis- *versus* conrotatory ring-opening at low forces gets transmuted at sufficiently high forces such that first, one transition state common to both dis- and conrotatory pathways is encountered followed by a first downhill bifurcation that decides about dis- and conrotatory ring-opening and, subsequently, by two additional separate downhill bifurcations for left/right migration.

The two topologically distinct low- and high-force energy landscapes are separated from each other by a cusp catastrophe, which happens at a critical force  $F_0^{\text{crit}}$  of roughly 1.6 nN in the present case. Analysis of the energy profiles as a function of external force in conjunction with topological analysis reveals that disrotatory ring-opening is energetically preferred below  $F_0^{\text{crit}}$  down to the zero force limit (where it becomes the Woodward-Hoffmann allowed electrocyclic reaction), whereas the conrotatory and disrotatory processes possess the same transition

state in the high force limit beyond  $F_0^{\text{crit}}$ . Thus, we find here that it is an intricate topological catastrophe that underlies and therefore explains the previously predicted<sup>27</sup> change in the ring-opening mechanism of *trans-gem*-dichlorocyclopropanes at about 1.6 nN in accord with subsequent single-molecule force spectroscopy experiments.<sup>28</sup>

In more general terms, sequential transition states and the branching of reaction pathways *via* bifurcations that lead to multiple product channels are well known in the study of chemical reactivity. Here, we show that both uphill and downhill bifurcations being pre- and post-transition-state features, respectively, can be shifted *continuously* by applying external mechanical forces as typically generated by sonication techniques. These changes can be merely quantitative in certain force regimes, but they can also qualitatively change the topology of the energy landscape that describes the process, for instance by shifting an uphill bifurcation over transition states to the downhill side. Beyond the specific case, the present findings delineate an approach towards steering the selectivity of chemical reactions in favor of desired products by means of mechanochemical activation.

### IV. METHODS

Optimization of both, transition states and IRCs of the four halogen-substituted cyclopropane derivatives have been performed using the unrestricted BLYP density functional and the TZVP basis set as implemented in Gaussian 09.<sup>39</sup> For the specific case of the dichloro cyclopropane derivative investigated in this study, good agreement between BLYP and CASSCF calculations can be observed as demonstrated in the SI of Ref. 27 and supported by previous benchmark calculations for bond breaking in mechanochemical reactions.<sup>40</sup> In addition, the NEVPT2 calculations in Sec. 1.2 of the SI of the present work for the difluoro species support this conclusion. A detailed description of the computational methods can be found in Sec. 1.3 of the SI. The force-transformed potential energy landscapes (FT-PES) have been generated by means of *ab initio* molecular dynamics simulations<sup>41</sup> on the basis of the Car-Parrinello method.<sup>42</sup> The reduced-dimensionality versions (FT-ePES) have been analyzed in terms of reaction pathways, not only including transition states but also bifurcation points, with the help of the so-called Dijkstra algorithm,<sup>36</sup> thus providing what we call Dijkstra paths. An extensive discussion of the respective computational details can be found in Sects. 1.5 and 1.6 of the SI.

### V. ACKNOWLEDGEMENT

It gives us pleasure to thank Przemyslaw Dopieralski and Michael Römelts for helpful discussions. We gratefully acknowledge generous financial support by the Rein-

hart Koselleck Grant "Understanding Mechanochemistry" (DFG MA 1547/9) as well as computer resources at HLRS Stuttgart, BOVILAB@RUB, and RV-NRW.

- <sup>1</sup>D. H. Ess, S. E. Wheeler, R. G. Iafe, L. Xu, N. Çelebi-Ölçim, and K. N. Houk, *Angew. Chem. Int. Ed.* **47**, 7592 (2008).
- <sup>2</sup>J. Rehbein and B. K. Carpenter, *Phys. Chem. Chem. Phys.* **13**, 20906 (2011).
- <sup>3</sup>G. B. Jones and P. M. Warner, *J. Am. Chem. Soc.* **123**, 2134 (2001).
- <sup>4</sup>J. Limanto, K. S. Khuong, K. N. Houk, and M. L. Snapper, *J. Am. Chem. Soc.* **125**, 16310 (2003).
- <sup>5</sup>F. Wang, A. Habtemariam, E. P. L. v. d. Geer, R. Fernández, M. Melchart, R. J. Deeth, R. Aird, S. Guichard, F. P. A. Fabbiani, P. Lozano-Casal, I. D. H. Oswald, D. I. Jodrell, S. Parsons, and P. J. Sadler, *Proc. Natl. Acad. Sci. U.S.A.* **102**, 18269 (2005).
- <sup>6</sup>T. Katori, S. Itoh, M. Sato, and H. Yamataka, *J. Am. Chem. Soc.* **132**, 3413 (2010).
- <sup>7</sup>M. K. Beyer and H. Clausen-Schaumann, *Chem. Rev.* **105**, 2921 (2005).
- <sup>8</sup>M. M. Caruso, D. A. Davis, Q. Shen, S. A. Odom, N. R. Sottos, S. R. White, and J. S. Moore, *Chem. Rev.* **109**, 5755 (2009).
- <sup>9</sup>J. Ribas-Ariño and D. Marx, *Chem. Rev.* **112**, 5412 (2012).
- <sup>10</sup>T. Stauch and A. Dreuw, *Chem. Rev.* **116**, 14137 (2016).
- <sup>11</sup>M. T. Ong, J. Leiding, H. Tao, A. M. Virshup, and T. J. Martínez, *J. Am. Chem. Soc.* **131**, 6377 (2009).
- <sup>12</sup>J. Ribas-Ariño, M. Shiga, and D. Marx, *Angew. Chem.* **121**, 4254 (2009).
- <sup>13</sup>P. Yu, A. Patel, and K. N. Houk, *J. Am. Chem. Soc.* **137**, 13518 (2015).
- <sup>14</sup>P. Yu, T. Q. Chen, Z. Yang, C. Q. He, A. Patel, Y.-h. Lam, C.-Y. Liu, and K. N. Houk, *J. Am. Chem. Soc.* **139**, 8251 (2017).
- <sup>15</sup>P. Valtazanos and K. Ruedenberg, *Theor. Chem. Acc.* **69**, 281 (1986).
- <sup>16</sup>J. Baker and P. M. W. Gill, *J. Comput. Chem.* **9**, 465 (1988).
- <sup>17</sup>W. Quapp and V. Melnikov, *Phys. Chem. Chem. Phys.* **3**, 2735 (2001).
- <sup>18</sup>L. Windhorn, J. S. Yeston, T. Witte, W. Fuß, M. Motzkus, D. Proch, K.-L. Kompa, and C. B. Moore, *J. Chem. Phys.* **119**, 641 (2003).
- <sup>19</sup>B. Lasorne, G. Dive, and M. Desouter-Lecomte, *J. Chem. Phys.* **122**, 184304 (2005).
- <sup>20</sup>W. Quapp, *J. Mol. Struct.* **695–696**, 95 (2004).
- <sup>21</sup>J. M. Lenhardt, A. L. Black, and S. L. Craig, *J. Am. Chem. Soc.* **131**, 10818 (2009).
- <sup>22</sup>J. M. Lenhardt, M. T. Ong, R. Choe, C. R. Evenhuis, T. J. Martínez, and S. L. Craig, *Science* **329**, 1057 (2010).
- <sup>23</sup>P. Dopieralski, J. Ribas-Ariño, and D. Marx, *Angew. Chem. Int. Ed.* **50**, 7105 (2011).
- <sup>24</sup>S. Akbulatov, Y. Tian, and R. Boulatov, *J. Am. Chem. Soc.* **134**, 7620 (2012).
- <sup>25</sup>H. M. Klukovich, T. B. Kouznetsova, Z. S. Kean, J. M. Lenhardt, and S. L. Craig, *Nature Chem.* **5**, 110 (2013).
- <sup>26</sup>J. Wang, T. B. Kouznetsova, Z. S. Kean, L. Fan, B. D. Mar, T. J. Martínez, and S. L. Craig, *J. Am. Chem. Soc.* **136**, 15162 (2014).
- <sup>27</sup>M. Wollenhaupt, M. Krupička, and D. Marx, *ChemPhysChem* **16**, 1593 (2015).
- <sup>28</sup>J. Wang, T. B. Kouznetsova, Z. Niu, M. T. Ong, H. M. Klukovich, A. L. Rheingold, T. J. Martínez, and S. L. Craig, *Nature Chem.* **7**, 323 (2015).
- <sup>29</sup>J. Wang, T. B. Kouznetsova, and S. L. Craig, *J. Am. Chem. Soc.* **137**, 11554 (2015).
- <sup>30</sup>J. Wang, M. T. Ong, T. B. Kouznetsova, J. M. Lenhardt, T. J. Martínez, and S. L. Craig, *J. Org. Chem.* **80**, 11773 (2015).
- <sup>31</sup>J. Wang, T. B. Kouznetsova, R. Boulatov, and S. L. Craig, *Nat. Commun.* **7**, 13433 (2016).
- <sup>32</sup>J. Wang, T. B. Kouznetsova, and S. L. Craig, *J. Am. Chem. Soc.* **138**, 10410 (2016).
- <sup>33</sup>S. J. Getty, D. A. Hrovat, and W. T. Borden, *J. Am. Chem. Soc.* **116**, 1521 (1994).
- <sup>34</sup>F. Tian, S. B. Lewis, M. D. Bartberger, W. R. Dolbier, and W. T. Borden, *J. Am. Chem. Soc.* **120**, 6187 (1998).
- <sup>35</sup>S. Maeda, Y. Harabuchi, Y. Ono, T. Taketsugu, and K. Morokuma, *Int. J. Quantum Chem.* **115**, 258 (2015).
- <sup>36</sup>E. Dijkstra, *Numer. Math.* **1**, 269 (1959).
- <sup>37</sup>R. Gilmore, *Catastrophe theory for scientists and engineers*, Vol. 2 (John Wiley&Sons, New York, 1981).
- <sup>38</sup>J. Ribas-Ariño, M. Shiga, and D. Marx, *J. Am. Chem. Soc.* **132**, 10609 (2010).
- <sup>39</sup>M. J. Frisch and et al., "Gaussian 09 Revision C.01," Gaussian Inc. Wallingford CT 2009, <http://www.gaussian.com>.
- <sup>40</sup>M. F. Iozzi, T. Helgaker, and E. Uggerud, *Mol. Phys.* **107**, 2537 (2009).
- <sup>41</sup>D. Marx and J. Hutter, *Ab Initio Molecular Dynamics: Basic Theory and Advances* (Cambridge University Press, 2009).
- <sup>42</sup>R. Car and M. Parrinello, *Phys. Rev. Lett.* **55**, 2471 (1985).